# Rydberg magnetoexcitons in Cu₂O quantum wells

David Ziemkiewicz ●,* Gerard Czajkowski, Karol Karpiński ●, and Sylwia Zielińska-Raczyńska ●

*Institute of Mathematics and Physics, UTP University of Science and Technology, Aleje Profesora Sylwestra Kaliskiego 7, 85-789 Bydgoszcz, Poland*

We present a theoretical approach that allows for calculation of optical functions for a Cu₂O quantum well (QW) with Rydberg excitons, in an external magnetic field of an arbitrary strength. Both Faraday and Voigt configurations are considered in the energetic region of *p* excitons. We use the real density matrix approach and an effective electron-hole potential, which enable us to derive analytical expressions for the QW magneto-optical functions. For both configurations, all three field regimes—weak, intermediate, and high field—are considered and treated separately. With the help of the developed approximation method we are able to estimate the limits between the field regimes. The obtained theoretical magnetoabsorption spectra show a good agreement with available experimental data.

## I. INTRODUCTION

The discovery of Rydberg excitons (REs) in cuprous oxide, first observed by Kazimierczuk *et al.* [1], initiated a large number of studies on their spectroscopic and optical properties (see the review paper, Ref. [2], where an extensive list of references can be found). In a majority of semiconductors, the observation of high exciton states is typically prevented by a small Rydberg energy of a few meV (e.g., 4.2 meV in the generic semiconductor GaAs with $n = 3$ as the highest observed state). Cuprous oxide stands out in this respect because it features a comparably large Rydberg energy of 90 meV, which together with narrow absorption lines provides well-suited conditions for exciting excitonic Rydberg states. These states are characterized by small binding energies, which makes them very sensitive to external fields. A lot of attention has been devoted to the interaction of REs with an external electric and/or magnetic field [3–8] (Stark and Zeeman effects), but most studies, both experimental and theoretical, concentrate on bulk crystals or plane-parallel slabs with dimensions much greater than the incident wave length and the effective Bohr radius.

In low-dimensional systems, due to confinement effects, the excitonic states have larger energies and oscillator strengths as compared with the bulk. This is also true for systems with REs; the states with a large main quantum number gain additional energy, and therefore one can expect that depending on the type of confinement, new states can appear, originating from the overlapping of confinement states with the Coulomb states and possibly resulting from Zeeman splitting in an external magnetic field. Recently, Cu₂O-based nanostructures with REs have awoken the interest of several groups [9–12], because one can expect interesting quantum effects to arise from competition between the geometric confinement, the excitons' motion, and their interaction with

additional external fields. This interest is also motivated by potential application benefits because quantum-confined structures with REs might be of use in practice for a new class of miniaturized, optoelectronic devices. From a practical point of view, one has to mention that devices such as lasers, photodetectors, modulators, and switches based on quantum wells turned out to be significantly faster than conventional electrical components, which is very desirable for telecommunication applications.

Similarly to the bulk case, the application of external fields to nanostructures changes the spectra of REs [9]. The electro- and magneto-optical properties of the typically studied cases such as GaAs-based nanostructures have been explored for decades, recently touching new areas such as magneto-optical properties of monolayer transition in metallic dichalcogenides [13]. The discussion of Cu₂O, when multiple Rydberg exciton states must be taken into account, is at its infancy. Here, we will consider the effect of an external magnetic field on a quantum well with Rydberg excitons. The effects of a geometric confinement are superimposed on REs' interaction with external fields and manifest in an intrinsic difference in magneto-optical spectra in terms of state energies, which in turn depend on field orientation. Inspired by the recent developments in the area of REs, we aim to analyze the magneto-optical properties of a Cu₂O-based quantum well (QW) in two different field orientations, namely, the Faraday and Voigt configurations. Both cases have been investigated experimentally for bulk Cu₂O crystals with RE for weak magnetic field (up to 4 T), and the numerical excitonic spectra were shown [3].

We will use the real density matrix approach (RDMA) to calculate the optical functions of a single Cu₂O QW with REs. This approach turned out to be successful in describing the optical properties of Cu₂O bulk crystals, including effects of external fields (Ref. [8] and references therein). The RDMA, adopted for bulk semiconductors by Stahl, Balslev, and others [14], has been then extended to low-dimensional systems (see Refs. [15–18]). In those works the attention was

*david.ziemkiewicz@utp.edu.pl

focused on nanostructures based on group II-VI [15,16,18] and III-V [17] semiconductors, with a prevalent role of *s* excitons affecting the optical properties. As has been shown in our recent paper [9], it is possible to extend the RDMA method to low-dimensional systems for $Cu_2O$-based nanostructures (in particular, quantum wells), where a different symmetry due to *p* excitons and the multiplicity of Rydberg exciton states must be taken into account. When describing the magneto-optical properties of the systems with excitons, one is confronted with well-known difficulties. The exciton, being an analogy of a hydrogen atom, is created and maintained by a Coulomb attraction, having a spherical symmetry. On the other hand, in the case of a quantum well a magnetic field and the confinement potentials have a cylindrical symmetry. These geometrical discrepancies rule out an analytical solution of the Schrödinger equation with the appropriate form of the Hamiltonian for the problem. To circumvent such obstacles, we have to use, as in the bulk case, various approximations, which depend on the relation between the exciton binding energy and the magnetic field energy. When the excitonic energies are larger than the magnetic field energies (the Landau state energies), we use the so-called weak-field approximation. In the opposite case, when the Landau state energies are greater than the excitonic state energies, we have to consider a high-field approximation. Between these two regions, one has to consider the intermediate-field case, when the excitonic energies and Landau state energies are comparable. Moreover, each magnetic field regime requires a different theoretical approach, and there is a strong need for a versatile estimation of how to designate the regime of the magnetic field; we propose a method which allows us to discern these regimes. When considering the magneto-optical properties of excitons in a QW, one has to account for effects related to the direction of the applied magnetic field. One distinguishes between the Faraday configuration, when the magnetic field is directed along the growth axis (the *z* axis, perpendicular to the planes of the QW), and the Voigt configuration, when the magnetic field is perpendicular to the *z* axis and parallel to the planes of the QW. We will show below that all the abovementioned effects can be described within the RDMA.

The paper is organized as follows. In Sec. II we recall the basic equations of the RDMA, adapted to the case of QWs, when external fields are applied. In Sec. III we explicitly derive the formulas for magnetosusceptibility for $Cu_2O$ QWs when the external magnetic field is applied in the Faraday configuration. We separately discuss the cases of a weak field (Sec. III A), a high field (Sec. III B), and an intermediate magnetic field (Sec. III C). Then we also consider three different regimes of the magnetic field strength in the case of the Voigt configuration (Secs. IV A–IV C). Section V contains illustrative numerical results and the description of a simple but effective method which allows for estimation of magnetic field regimes, while a summary and the conclusions of our paper are presented in Sec. VI. Appendixes A–D contain the details of the analytical calculations.

## II. BASIC EQUATIONS

We will use the real density matrix approach, applied to a single quantum well with Rydberg states, similarly as was

done for low-dimensional structures in Ref. [9]. In this approach the optical properties are described by an equation for the two-point correlation function $Y_{12}$ (also called the coherent amplitude) of the electron-hole pair of coordinates $\mathbf{r}_1 = \mathbf{r}_h$ and $\mathbf{r}_2 = \mathbf{r}_e$, which for a pair of conduction and valence bands reads

$$-i(\hbar\partial_t + \Gamma)Y_{12} + H_{eh}Y_{12} = \mathbf{M}\mathbf{E}, \qquad (1)$$

where $\mathbf{E}$ is the electric vector of the electromagnetic wave propagating in QW, $\Gamma$ is a phenomenological damping coefficient, and $\mathbf{M}(\mathbf{r})$ is a smeared-out transition dipole density which depends on the coherence radius $r_0 = [(2\mu/\hbar^2)E_g]^{-1/2}$ ($E_g$ is the fundamental gap; $\mu$ is the reduced effective mass of the electron-hole pair, and $\mathbf{r}$ is the relative electron-hole distance) [19]. Specific forms of $\mathbf{M}(\mathbf{r})$ will be defined in subsequent sections.

The RDMA is a mesoscopic approach, which in the lowest order neglects all effects from the multiband semiconductor structure, so that the exciton Hamiltonian becomes identical to the two-band effective mass Hamiltonian $H_{eh}$, which in the case when external fields are applied includes the electron and hole kinetic energy, the electron-hole interaction potential, the terms related to the external fields, and the confinement potentials [20]. As a consequence, the Hamiltonian $H$ is given by

$$\begin{aligned} H = E_g &+ \frac{1}{2m_e}\left(\mathbf{p}_e - e\frac{\mathbf{r}_e \times \mathbf{B}}{2}\right)^2 \\ &+ \frac{1}{2m_h}\left(\mathbf{p}_h + e\frac{\mathbf{r}_h \times \mathbf{B}}{2}\right)^2_z \\ &+ \frac{1}{2m_h}\left(\mathbf{p}_h + e\frac{\mathbf{r}_h \times \mathbf{B}}{2}\right)^2_\parallel + e\mathbf{F} \cdot (\mathbf{r}_e - \mathbf{r}_h) \\ &+ V_{\mathrm{conf}}(\mathbf{r}_e, \mathbf{r}_h) - \frac{e^2}{4\pi\epsilon_0\epsilon_b|\mathbf{r}_e - \mathbf{r}_h|}, \end{aligned} \qquad (2)$$

where $\mathbf{B}$ is the magnetic field vector, $\mathbf{F}$ is the vector of the external electric field, $V_{\mathrm{conf}}$ are the surface potentials for electrons and holes, $\epsilon_b$ is the background dielectric constant, $m_{hz}, m_{h\parallel}$ are the components of the hole effective mass tensor, and the electron mass is assumed to be isotropic. The total polarization of the medium is related to the coherent amplitude by

$$\mathbf{P}(\mathbf{R}) = 2\,\mathrm{Re}\int d^3r\,\mathbf{M}(\mathbf{r})Y(\mathbf{R}, \mathbf{r}), \qquad (3)$$

where $\mathbf{R}$ is the center-of-mass coordinate. This, in turn, is used in Maxwell's field equation

$$c^2\nabla^2\mathbf{E}(\mathbf{R}) - \epsilon_b\ddot{\mathbf{E}} = \frac{1}{\epsilon_0}\ddot{\mathbf{P}}(\mathbf{R}). \qquad (4)$$

Equations (1), (3), and (4) form a system of coupled integrodifferential equations. In the bulk limits, they can be transformed into Fredholm integral equations of the second kind, with certain nonlocal integral kernels. Their solution is a nontrivial task. The problem becomes simpler in the quantum well limit. With the help of the long-wave approximation, one

arrives at the mean effective quantum well susceptibility

$$\chi = \frac{1}{L} \int_{-L/2}^{L/2} \frac{P(Z)}{\epsilon_0 E(Z)} dZ. \tag{5}$$

From the Maxwell equation (4), one can calculate the mean effective dielectric function $\epsilon = \epsilon_b + \chi$ and the absorption coefficient

$$\alpha = 2\frac{\hbar\omega}{\hbar c} \text{Im}\sqrt{\epsilon_b + \chi}. \tag{6}$$

The detailed form of the Hamiltonian for both Faraday and Voigt configurations will be applied in the following sections. The detailed calculations are presented in the Appendixes and Ref. [21].

## III. THE FARADAY CONFIGURATION

When the magnetic field **B** is applied to a QW in the growth direction, which we identify with the $z$ axis, we deal with the Faraday configuration.

### A. Weak-field limit

In this configuration we will consider the optical response of a QW with thickness $L$ to a normally incident electromagnetic wave. The QW is located in the $x$-$y$ plane, with the surfaces at $z = \pm L/2$. We can separate the motion in the $z$ direction (where the particles are treated separately) from the in-plane motion where we use the relative and exciton center-of-mass coordinates. In the case of $F = 0$ we transform the Hamiltonian (2) into the form

$$\begin{aligned} H = E_g &- \frac{\hbar^2}{2m_e}\frac{\partial^2}{\partial z_e^2} - \frac{\hbar^2}{2m_h}\frac{\partial^2}{\partial z_h^2} \\ &+ \frac{\mathbf{p}_\parallel^2}{2\mu} + \frac{\mathbf{P}_\parallel^2}{2M_\parallel} + \frac{1}{8}\mu\omega_c^2 r_\parallel^2 + \frac{e}{2\mu'}B\mathcal{L}_z \\ &- \frac{e}{M_\parallel}\mathbf{P}_\parallel \cdot (\mathbf{r}_\parallel \times \mathbf{B}) + V_{\text{conf}}(\mathbf{r}_e, \mathbf{r}_h), \end{aligned} \tag{7}$$

where $\omega_c = eB/\mu_\parallel$ is the cyclotron frequency and the reduced mass $\mu'$ is defined as

$$\frac{1}{\mu'} = \frac{1}{m_e} - \frac{1}{m_h}. \tag{8}$$

The operator $\mathcal{L}_z$ is the $z$ component of the angular momentum operator.

We assume a parabolic confinement in the $z$ direction,

$$V_{\text{conf}} = \frac{1}{2}m_e\omega_{ez}^2 z_e^2 + \frac{1}{2}m_h\omega_{hz}^2 z_h^2. \tag{9}$$

The quasiparticles (electron and hole) move independently in such a potential and have different confinement energies. When the confinement parameters $\omega_{ez}, \omega_{hz}$ are equal, the sum of their energies represents the exciton center-of-mass quantized states.

Using the notation

$$H_{m,\omega}^{(1D)}(z) = \frac{p_z^2}{2m} + \frac{1}{2}m\omega^2 z^2, \tag{10}$$

the QW Hamiltonian can be written in the form

$$\begin{aligned} H_{\text{QW}} = E_g &+ H_{m_e, \omega_{ez}}^{(1D)}(z_e) + H_{m_h, \omega_{hz}}^{(1D)}(z_h) \\ &- \frac{\hbar^2}{2M_\parallel}\nabla_{R_\parallel}^{(2D)2} - \frac{\hbar^2}{2\mu}\nabla_r^{(2D)2} \\ &- \frac{\mu}{\mu'}i\gamma R^* \partial_\phi + \frac{R^*}{4a^{*2}}\gamma^2 r^2 + V_{eh}, \end{aligned} \tag{11}$$

where $V_{eh}$ is the electron-hole Coulomb interaction potential, $a^*$ is the exciton Bohr radius and $R^*$ the exciton Rydberg energy, $\nabla_{R_\parallel}^{(2D)2}, \nabla_r^{(2D)2}$ denote two-dimensional nabla operators, and $r = \sqrt{x^2 + y^2}$. The dimensionless strength of the magnetic field $\gamma$ is defined as

$$\gamma = \hbar\omega_c/2R^*. \tag{12}$$

In the weak-magnetic-field limit, excitons play a dominant role in determining the optical response, and the magnetic field can be treated as a perturbation [8]; we use the two-dimensional Coulomb potential

$$V_{eh} = -\frac{e^2}{4\pi\epsilon_0\epsilon_b r}. \tag{13}$$

We consider the two-dimensional approximation with the following justification. First, we are more interested in the magnetic field effects than in the accuracy of eigenvalues. Second, we want to account for higher excitonic states where, for $p$ symmetry, the spatial extension of the exciton wave function increases approximately as $j^2$. The extension of higher states can be larger (or even much larger) than the quantum well thickness $L$, thus satisfying the condition for narrow QWs. In addition, the energy values for higher excitonic states differ only slightly from those of a three-dimensional system, and the difference between two- and three-dimensional calculations affects mostly the oscillator strengths. The two-dimensional potential allows for analytical calculations with inclusion of arbitrary high exciton states (which is the key point for Rydberg excitons), whereas more accurate calculations (for example, variational) can be performed only for the lowest or the lowest few exciton states. For these reasons we use the two-dimensional Coulomb potential (13).

With respect to the above assumptions, the left-hand-side operator in Eq. (11) includes two one-dimensional harmonic-oscillator Hamiltonians and the two-dimensional Coulomb Hamiltonian

$$H_{\text{Coul}}^{(2D)} = -\frac{\hbar^2}{2\mu}\nabla_r^{(2D)2} - \frac{e^2}{4\pi\epsilon_0\epsilon_b r}. \tag{14}$$

We also neglect the terms related to the in-plane center-of-mass motion. Therefore the solution for the amplitude $Y$ can be expressed in terms of eigenfunctions of the abovementioned Hamiltonians

$$Y_{jmN_eN_h} = \sum_{N_e, N_h, j, m} c_{jmN_eN_h} \psi_{\alpha_{ez,N_e}}^{(1D)}(z_e) \psi_{\alpha_{hz,N_h}}^{(1D)}(z_h) \psi_{jm}(r, \phi), \tag{15}$$

where $\psi_{\alpha_z,N}^{(1D)}(z)$ ($N_e, N_h = 0, 1, \ldots$) are the quantum oscillator eigenfunctions for electron and hole, respectively.

$$\psi_{\alpha_z,N_{e,h}}^{(1D)}(z) = \pi^{-1/4}\sqrt{\frac{\alpha_z}{2^N_{e,h} N_{e,h}!}} H_N(\alpha_z z)e^{-\frac{\alpha_z^2}{2}z^2},$$

$$\alpha_z = \sqrt{\frac{m_{e,h}\omega_z}{\hbar}}, \tag{16}$$

$H_N(x)$ are Hermite polynomials ($N_{e,h} = 0, 1, \ldots$), $m_{e,h}$ are the electron (hole) effective masses, and $\psi_{jm}(\rho, \phi)$ are the eigenfunctions of the two-dimensional Hamiltonian (14)

$$\psi_{jm}(\rho, \phi) = R_{jm}(\rho)\frac{e^{im\phi}}{\sqrt{2\pi}},$$

$$R_{jm} = A_{jm}e^{-2\lambda\rho}(4\lambda\rho)^{|m|}L_j^{|2m|}(4\lambda\rho),$$

$$\lambda = \frac{1}{1 + 2(j + |m|)},$$

$$A_{jm} = \frac{4}{(2j + 2|m| + 1)^{3/2}}\left[\frac{j!}{(j + 2|m|)!}\right]^{1/2}, \tag{17}$$

where $L_n^\alpha(x)$ are the Laguerre polynomials, for which we use the definition

$$L_n^\alpha(x) = \binom{n + \alpha}{n}M(-n, \alpha + 1; x),$$

with the Kummer function $M(a, b, z)$ (the confluent hypergeometric function) [22], and $\rho = r/a^*$ is the scaled space variable. Here, we use the transition dipole density in the form [8]

$$M(\boldsymbol{\rho}, z_e, z_h) = \frac{M_0}{2\rho_0^3}\rho\, e^{-\rho/\rho_0}\frac{e^{i\phi}}{\sqrt{2\pi}}\delta(z_e - z_h), \tag{18}$$

with the integrated strength $M_0$ and the coherence radius $\rho_0 = r_0/a^*$, where $r_0 = \sqrt{\frac{\hbar^2}{2\mu E_g}}$. The coefficient $M_0$ and the coherence radius $\rho_0$ are connected through the longitudinal-transversal energy $\Delta_{LT}$ [19]

$$(M_0\rho_0)^2 = \frac{4}{3}\frac{\hbar^2}{2\mu}\epsilon_0\epsilon_b a^*\frac{\Delta_{LT}}{R^*}e^{-4\rho_0}. \tag{19}$$

The calculation of the QW susceptibility, from which other optical functions can be determined, consists of several steps. First, we assume that the incident electromagnetic wave is linearly polarized with the electric vector **E** having a component in the direction $\alpha$ and an amplitude $\mathcal{E}$; the dipole density vector **M** has a component $M$ in the form (18) in the same direction. Then, with the help of Eqs. (3) and (5), applying the long-wave approximation, we calculate the mean QW susceptibility from the formula

$$\chi = \frac{2}{\epsilon_0\mathcal{E}}\frac{1}{L}\int_{-L/2}^{L/2}dz_e dz_h\int_0^\infty d\rho\,\rho\int_0^{2\pi}d\phi\,M(\boldsymbol{\rho}, z_e, z_h)$$

$$\times Y(\boldsymbol{\rho}, z_e, z_h). \tag{20}$$

The first step to calculate $\chi$ is to determine the exciton amplitude $Y$. Finally, we use Eq. (1) with the Hamiltonian given by Eq. (11). Inserting the expansion (15) into Eq. (1) and making use of the dipole density in the form (18), one obtains a set

of linear algebraic equations for the expansion coefficients $c_{jmN_eN_h}$

$$\sum_{\ell=0}^{j_{max}} a_{j\ell mN_eN_h}c_{\ell mN_eN_h} = b_{j1}\delta_{N_eN_h}\mathcal{E},$$

$$a_{j\ell mN_eN_h} = \delta_{j\ell}\kappa_{jmN_eN_h}^2 + V_{j\ell m},$$

$$\kappa_{jmN_eN_h}^2 = \frac{1}{R^*}\left(E_g - \hbar\omega - i\Gamma + \varepsilon_{jm}R^* + W_{eN_e}\right.$$

$$\left. + W_{hN_h} + \frac{\mu}{\mu'}m\gamma\,R^*\right),$$

$$\epsilon_{jm} = -4\lambda_{jm}^2,$$

$$\lambda_{jm} = \frac{1}{2j + 2|m| + 1},$$

$$b_{j|m|N_eN_h} = b_{j1N_eN_h}$$

$$= \sqrt{\frac{(j + 1)(j + 2)}{(j + 3/2)^5}}(1 + 2\rho_0\lambda_{j1})^{-4}$$

$$\times F\left(-j, 4; 3; \frac{1}{s}\right)$$

$$s = \frac{1 + 2\rho_0\lambda_{jm}}{4\rho_0\lambda_{jm}},$$

$$j, \ell = 0, 1, 2, \ldots, j_{max}, \quad m = \pm 1,$$

$$N_e, N_h = 0, 1, 2, \ldots, \tag{21}$$

where $F(\alpha, \beta; \gamma; z)$ is a hypergeometric series. $V_{j\ell m}$ are matrix elements

$$V_{j\ell m} = \tfrac{1}{4}\gamma^2\langle R_{jm}(\rho)|\rho^2|R_{\ell m}(\rho)\rangle, \tag{22}$$

and their detailed form is given by Eq. (A4) in Appendix A. The $z$-confinement energies $W_{eN_e}, W_{hN_h}$ and the parameters $\alpha$ are defined as follows:

$$\alpha_e = \sqrt{\frac{m_e}{\mu}}\sqrt{\frac{W_{e0}}{R^*}},$$

$$\alpha_h = \sqrt{\frac{m_h}{\mu}}\sqrt{\frac{W_{h0}}{R^*}},$$

$$p = \frac{1}{2}(\alpha_{ez}^2 + \alpha_{hz}^2),$$

$$W_{e0} = \left(\frac{\pi a_e^*}{L}\right)^2 R_e^*,$$

$$W_{h0} = \left(\frac{\pi a_h^*}{L}\right)^2 R_h^*,$$

$$W_{e1} = 3\,W_{e0},$$

$$W_{h1} = 3\,W_{h0}.$$

For the case $\alpha_e = \alpha_h = \alpha^F = \pi/L$ the specific values of these parameters are

$$p = 1,$$

$$W_{e0} = \left(\frac{\pi a_e^*}{L}\right)^2 R_e^*,$$

$$W_{h0} = \left(\frac{\pi a_h^*}{L}\right)^2 R_h^*,$$

$$\frac{W_{e0} + W_{h0}}{R^*} = \left(\frac{\pi a^*}{L}\right)^2 =: \frac{W_{eh0}}{R^*},$$

$$\frac{W_{e1} + W_{h1}}{R^*} = \frac{3\,W_{eh0}}{R^*},$$

$$\frac{W_{eN} + W_{hN}}{R^*} = \frac{(2N+1)\,W_{eh0}}{R^*}.$$

With the above definitions, taking $N_e = N_h = N$ with computed $c$ coefficients, we use them in the expansion (15), which is in turn inserted into Eq. (20), from which we calculate the mean QW magnetosusceptibility for the Faraday configuration

$$\chi^F(\omega) = 48\epsilon_b \frac{\Delta_{LT}}{R^*}\left(\frac{a^*}{L}\right) \sum_{j=0}^{\mathcal{N}} b_{j1}[\langle\Psi_{00}\rangle_L (c_{j100} + c_{j-100})$$

$$+ \langle\Psi_{11}\rangle_L (c_{j111} + c_{j-111}) + \cdots \langle\Psi_{NN}\rangle_L$$

$$\times (c_{j1NN} + c_{j-1NN})]\langle\Psi_{NN}\rangle_L$$

$$= \frac{1}{2^N N!}\frac{2}{\sqrt{\pi}}\int_0^{\alpha L/2} e^{-t^2} H_N^2(t)\,dt. \tag{23}$$

### B. High-field limit

In the high-field limit, the magnetic energy contributions to the Hamiltonian are much greater than the Coulomb one, and the energies of Landau states are larger than the absolute value of the lowest exciton state. Therefore we seek solutions for the exciton amplitude $Y$ in terms of the eigenfunctions of the "kinetic + magnetic + confinement" part of the Hamiltonian (11).

$$Y = \sum_{nmN_eN_h} c_{nmN_eN_h} R_{nm}(\rho)\frac{e^{im\phi}}{\sqrt{2\pi}}\Psi_{N_eN_h}(z_e, z_h), \tag{24}$$

where

$$R_{nm}(\rho) = \sqrt{\gamma}\sqrt{\frac{n!}{(n+|m|)!}}\left(\frac{\gamma\rho^2}{2}\right)^{|m|/2} e^{-\gamma\rho^2/4} L_n^{|m|}\left(\frac{\gamma\rho^2}{2}\right), \tag{25}$$

$n = 0, 1, \ldots$ and $m$ characterize Landau states, and $L_n^{|m|}$ are associated Laguerre polynomials. Similarly as in the case of weak magnetic fields, we insert the expansion (24) into Eq. (1) with an appropriate form of the Hamiltonian $H$, to obtain the expansion coefficients $c$, which are calculated from the set of

linear equations

$$\sum_{nmN_eN_h} a_{n\ell mN_eN_h} c_{nmN_eN_h} = d_{\ell m}\delta_{N_eN_h},$$

$$a_{n\ell mN_eN_h} = \delta_{n\ell}\kappa_{nmN_eN_h}^2 + V_{n\ell m},$$

$$V_{n\ell m} = \langle R_{nm}|\left(-\frac{2}{\rho}\right)|R_{\ell m}\rangle,$$

$$d_{nm} = \langle R_{nm}\frac{e^{im\phi}}{\sqrt{2\pi}}|M(\rho, \phi)\rangle$$

$$= (M_0\rho_0)\frac{2\gamma}{\sqrt{\pi}}\sqrt{n+1}\frac{\left(1 - \frac{\gamma\rho_0^2}{2}\right)^n}{\left(1 + \frac{\gamma\rho_0^2}{2}\right)^{n+2}}, \tag{26}$$

where

$$\kappa_{nmN_eN_h}^2 = \frac{2\mu}{\hbar^2}a^{*2}(E_g - \hbar\omega - i\Gamma)$$

$$+ U_{nm}/R^* + \frac{W_{eN_e} + W_{hN_h}}{R^*},$$

$$U_{nm}/R^* = \gamma\left(2n + \mathrm{sgn}(B)m\frac{\mu}{\mu'} + |m| + 1\right). \tag{27}$$

The detailed form of the matrix elements $V_{n\ell m}$ is given by Eq. (A5) in Appendix A. With the help of the coefficients $c$ one can get the exciton amplitude $Y$, which is then substituted into Eq. (20), from which the mean magnetosusceptibility for the case of high magnetic fields can be determined. Restricting the considerations to the lowest confinement state in the $z$ direction and denoting $\kappa_{nm00} = \kappa_{nm}$, the magnetosusceptibility for the Faraday configuration for the high field is given by the following formula:

$$\chi^F = \frac{16}{3\pi}\epsilon_b\gamma^2\left(\frac{a^*}{L}\right)\frac{\Delta_{LT}}{R^*}e^{4\rho_0}\frac{\alpha_e\alpha_h}{p}$$

$$\times \mathrm{erf}\left(\frac{L\sqrt{p}}{2}\right)\sum_{n=0}^{N}\sum_{m} c_{nm}d_{n1},$$

$$d_{n1} = \sqrt{n+1}\exp\left[2\rho_0 - (n+1)\gamma\rho_0^2\right] = \sum_{n=0}^{n_{\max}} a_{n\ell m}c_{nm}. \tag{28}$$

### C. Intermediate fields

For intermediate magnetic fields, the exciton energies and the Landau states' energies are comparable, and therefore we must include both the contributions of Coulomb interaction and the magnetic field on the same footing. In Ref. [8] we developed a method for such calculations, and here we will recall its fundamental points. Equation (1) has to be transformed into the Lippmann-Schwinger equation in the scalar form for one dimension

$$H_{\mathrm{kin}+B+\mathrm{confine}}Y = ME - VY, \tag{29}$$

where $V$ is the two-dimensional Coulomb electron-hole (e-h) interaction potential, and $H_{\mathrm{kin}+B+\mathrm{confine}}$ is the "kinetic + magnetic + confinement" part of the Hamiltonian (7). The above

equation can be solved by means of the appropriate Green's function [23]

$$Y = GME - GVY. \qquad (30)$$

The Green's function has the form [23]

$$\begin{aligned}
&G(\rho, \rho'; \phi, \phi'; z_e, z'_e; z_h, z'_h) \\
&= \frac{1}{2\pi} \sum_{N_e, N_h} \sum_{n=0}^{\infty} \sum_m e^{im(\phi - \phi')} \psi^{(1D)}_{\alpha_h, N_h}(z_h) \psi^{(1D)}_{\alpha_h, N_h}(z'_h) \\
&\quad \times \psi^{(1D)}_{\alpha_e, N_e}(z_e) \psi^{(1D)}_{\alpha_e, N_e h}(z'_e) \frac{R_{nm}(\rho) R_{nm}(\rho')}{\kappa^2_{nmN_e N_h}},
\end{aligned}$$

where $R_{nm}(\rho)$ are given in Eq. (25) and $\kappa^2_{nmN_e N_h}$ is given by Eq. (27).

The Lippmann-Schwinger equation (29) is an integral equation for the unknown function $Y$. There are several methods to solve such equations. We choose the method of a trial function $Y$, which we take in the form

$$\begin{aligned}
Y &= \Psi_{00} R_{01}(\rho) \left[ \sum_{m=\pm 1} Y_{0m,00} \exp(-\kappa_{0m00}\rho) \frac{e^{im\phi}}{\sqrt{2\pi}} \right] \\
&\quad + \sum_{n=1}^{\infty} \sum_{N_e, N_h \geqslant 1} \sum_m \frac{e^{im\phi}}{\sqrt{2\pi}} Y_{nmN_e N_h} R_{nm}(\rho) \Psi_{N_e N_h}, \quad (31)
\end{aligned}$$

where $Y_{nmN_e N_h}$ are coefficients to be determined and

$$\Psi_{N_e N_h} = \psi^{(1D)}_{\alpha_e, N_e}(z_e) \psi^{(1D)}_{\alpha_h, N_h}(z_h). \qquad (32)$$

The exciton amplitude $Y$, and thus the magnetosusceptibility, is known once the parameters $Y_{nmN_e N_h}$ are calculated, which is done in Appendix B. With $Y_{0\pm 1,00}$ given by (B2) substituted into Eqs. (31) and (20), we obtain the mean QW magnetosusceptibility in the Faraday configuration and intermediate-magnetic-field regime in the form

$$\begin{aligned}
\chi &= \frac{16}{3\pi} \epsilon_b \gamma^2 \left( \frac{a^*}{L} \right) \frac{\Delta_{LT}}{R^*} e^{4\rho_0} \frac{\alpha_e \alpha_h}{p} \operatorname{erf} \left( \frac{L\sqrt{p}}{2} \right) \\
&\quad \times \sum_{m=\pm 1} \left\{ \frac{3 d_{0m} \exp\left( \frac{u^2}{4} \right) D_{-4}(u)}{\exp(z^2/4) \left[ 3\kappa^2_{0m} D_{-4}(z) - 2\sqrt{\gamma} D_{-3}(z) \right]} \right. \\
&\quad \left. + \sum_{n=1}^{N} \frac{d^2_{nm}}{\kappa^2_{nm}} \right\}, \qquad (33)
\end{aligned}$$

$$\begin{aligned}
d_{nm} &= d_{n|m|} = \sqrt{n+1} \frac{\left( 1 - \gamma \rho_0^2/2 \right)^n}{\left( 1 + \gamma \rho_0^2/2 \right)^{n+2}} \\
&\approx \sqrt{n+1} \, e^{-(n+1)\gamma \rho_0^2},
\end{aligned}$$

$$u = \frac{\kappa_{0\pm 1}}{s}, \quad s = \frac{1}{\rho_0} \left( 1 + \frac{\gamma \rho_0^2}{2} \right)^{1/2}, \quad z = \frac{\kappa_{0\pm 1}}{\sqrt{\gamma}}.$$

## IV. THE VOIGT CONFIGURATION

In the Voigt configuration, the magnetic field is perpendicular to the wave vector of the propagating electromagnetic wave and, in the QW geometry, parallel to the QW planes. As in the case of the Faraday configuration, we will discuss the three regimes—the weak, intermediate, and high magnetic

field—with the proper form of the Hamiltonian for each of them.

### A. Weak-field regime

We choose the magnetic field **B** parallel to the $x$ axis, which corresponds to the vector potential $\mathbf{A} = \frac{B}{2}(0, -z, y)$. With this potential and the confinement potentials (9), the QW Hamiltonian (2) in the weak-field limit takes the form

$$\begin{aligned}
H^V_{QW} &= E_g + H^{(2D)}_{Coul} + H^{(1D)}_{m_e, \Omega_{ez}}(z_e) + H^{(1D)}_{m_h, \Omega_{hz}}(z_h) + H', \\
H' &= \frac{1}{8\mu} e^2 B^2 M_Y^2 + \frac{1}{8\mu} e^2 B^2 y^2 q + \frac{1}{4\mu'} e^2 B^2 M_Y y, \\
q &= \frac{m_h^2 - m_h m_e + m_e^2}{M^2}, \qquad (34)
\end{aligned}$$

where the relative and the center-of-mass coordinates $y$, $M_Y$ in the $y$ direction are introduced

$$M_Y = \frac{m_e y_e + m_h y_h}{M}, \quad y = y_e - y_h, \quad M = m_e + m_h.$$

We will proceed in a similar way as in the case of a weak field in the Faraday configuration. Treating the magnetic part $H'$ as a perturbation, we assume the solution for $Y$ in the form (15), with the eigenfunctions appropriate for the Hamiltonian (34). This leads to the system of equations (21) for the expansion coefficients $c$, where now the matrix elements are given by

$$V^{Voigt}_{jkm} = \tfrac{1}{2} q V^{Faraday}_{jkm}, \qquad (35)$$

with $V^{Faraday}_{jkm}$ defined in Eq. (A4).

The susceptibility is obtained in the form (23), where

$$\langle \Psi_{NN} \rangle_L = \frac{1}{2^N N!} \frac{2}{\sqrt{\pi}} \int_0^{\alpha^V L/2} e^{-t^2} H_N^2(t) dt,$$

$$\alpha_e^V = \alpha_h^V =: \alpha^V = \frac{1}{a^*} \left[ \frac{\gamma^2}{4} + \left( \frac{\pi a^*}{L} \right)^4 \right]^{1/4},$$

$$\frac{W^V_{e0}}{R^*} + \frac{W^V_{h0}}{R^*} = \frac{W^V_{eh0}}{R^*} = \left[ \frac{\gamma^2}{4} + \left( \frac{\pi a^*}{L} \right)^4 \right]^{1/2}, \qquad (36)$$

and for $N_e = N_h = N$, the confinement energies are now defined as

$$\begin{aligned}
W^V_{eN} + W^V_{hN} &= W_{NN} = (2N+1) W^V_{eh0}, \\
N &= 0, 1, 2, \ldots, N_{max}, \\
W^V_{eh0} &= \left[ \frac{\gamma^2}{4} + \left( \frac{\pi a^*}{L} \right)^4 \right]^{1/2} R^*. \qquad (37)
\end{aligned}$$

### B. High-field regime

In the high-field limit for the Voigt configuration the e-h Coulomb interaction is considered as a perturbation, so the unperturbed QW Hamiltonian has the form

$$\begin{aligned}
H^V_{QW} &= \frac{p_x^2}{2\mu} + H^{(1D)}_{\mu, \Omega_y}(y) + H^{(1D)}_{m_e, \Omega ez}(z_e) + H_{m_h, \Omega_{hz}}(z_h), \\
\frac{\hbar \Omega_y}{2R^*} &= \frac{\gamma}{2} \sqrt{q}, \qquad (38)
\end{aligned}$$

with $q$ defined in Eq. (34). We apply the method of the so-called adiabatic potentials (Ref. [8] and references therein). The exciton amplitude $Y$ will be assumed in the form

$$Y(x, y, z_e, z_h) = \sum_{N_x N_y N_e N_h} c_{N_x N_y N_e N_h} \psi_{N_x}(x) \psi_{\beta, \Omega_y}^{(1D)}(y) \Psi_{N_e N_h}(z_e, z_h),$$

(39)

where

$$\psi_{\beta, N_y}^{(1D)} = \pi^{-1/4} \sqrt{\frac{\beta}{2^{N_y} N_y!}} H_{N_y}(\beta y) e^{-\beta^2 y^2/2},$$

$$\beta = \frac{1}{a^*} \sqrt{\frac{\hbar \Omega_y}{2R^*}} = \frac{1}{a^*} q^{1/4} \sqrt{\frac{\gamma}{2}} = \frac{1}{a^*} \tilde{\beta},$$

$$\Psi_{N_e N_h}(z_e, z_h) = \psi_{\alpha_e^V, N_e}^{(1D)}(z_e) \psi_{\alpha_h^V, N_e}^{(1D)}(z_h),$$

(40)

and $\psi_{N_x}(x)$ are eigenfunctions of the operator

$$H_x = \frac{p_x^2}{2\mu} + V_{N_y N_y'}(x),$$

(41)

where

$$V_{N_y N_y'}(x) = -2 \int_{-\infty}^{\infty} dy \frac{\psi_{\beta, N_y}^{(1D)}(y) \psi_{\beta, N_y'}^{(1D)}(y)}{\sqrt{x^2 + y^2}}.$$

(42)

We restrict the discussion to the diagonal terms $V_{N_y N_y}$ and approximate expression (42) by

$$V_{N_y} = -\frac{2}{a_{N_y} + |x|}.$$

(43)

The coefficients $a_{N_y}$, for odd-parity eigenfunctions $\psi_{\beta, N_y}^{(1D)}$, $N_y = 2n + 1$, are calculated in Appendix C. In this approximation the Schrödinger equation with the operator (41) becomes

$$\left( \frac{p_x^2}{2\mu} - \frac{2}{a_{N_y} + |x|} \right) \psi = E \psi,$$

(44)

which gives the eigenfunctions

$$\psi_{jn}(x) = \frac{\sqrt{2}}{j+1} e^{-(|x| + a_{2n+1})/(j+1)} L_j^1 \frac{2(|x| + a_{2n+1})}{j+1},$$

(45)

$j = 0, 1, \ldots$, and eigenvalues $E_j = -\frac{R^*}{(j+1)^2}$. With the above functions we calculate the expansion coefficients in Eq. (39) and thus the exciton amplitude $Y$, and finally, we calculate the mean QW magnetosusceptibility for the Voigt configuration in the limit of high magnetic fields

$$\chi^V = \frac{4\sqrt{\pi}}{3} \epsilon_b \Delta_{LT} e^{4\rho_0} \sum_{j=0}^{N_x \max} \sum_{n=0}^{N_y \max} \sum_{N=0}^{N_z \max} \frac{2}{(j+1)^2}$$

$$\times e^{-\frac{2a_{2n+1}}{j+1}} \left[ L_j^{(1)} \left( \frac{2 a_{2n+1}}{j+1} \right) \right]^2$$

$$\times \left( \frac{2\tilde{\beta}}{1 + \tilde{\beta}^2 \rho_0^2} \right)^3 \frac{(2n+1)!}{2^{2n+1}(n!)^2} \left( \frac{1 - \tilde{\beta}^2 \rho_0^2}{1 + \tilde{\beta}^2 \rho_0^2} \right)^{2n}$$

$$\times \left[ E_g - \hbar\omega - \frac{R^*}{(j+1)^2} + \left( 2n + \frac{3}{2} \right) \hbar\Omega_y + W_{NN} \right]^{-1},$$

(46)

where $\langle \Psi_{NN} \rangle_L$ are defined in Eq. (36) and the confinement energies $W_{NN}$ are defined in Eq. (37).

### C. Intermediate fields

We calculate the mean magnetosusceptibility for the Voigt configuration and in the regime of intermediate magnetic fields by the Green's function method described above for the case of Faraday configuration. Again, we use the Lippmann-Schwinger equation (30) to calculate the exciton amplitude $Y$, which is then used to obtain the magnetosusceptibility. The Green's function in Eq. (30) satisfies, by definition, the equation

$$H^V G(x, x'; y, y'; z_e, z_e'; z_h, z_h')$$
$$= -\delta(x - x')\delta(y - y')\delta(z_e - z_e')\delta(z_h - z_h'),$$

where the operator $H^V$ has the form (38). Expressing the Green's function in terms of eigenfunctions of the operators contained in $H^V$, one obtains

$$G = \frac{2\mu}{\hbar^2} \sum_{n, N_e, N_h} \frac{1}{2\pi} \int_{-\infty}^{\infty} dk \, e^{ik(x-x')} \psi_{\beta, n}^{(1D)}(y) \psi_{\beta, n}^{(1D)}(y')$$

$$\times \frac{\psi_{\alpha_e^V, N_e}^{(1D)}(z_e) \psi_{\alpha_e^V, N_e}^{(1D)}(z_e') \psi_{\alpha_h^V, N_h}^{(1D)}(z_h) \psi_{\alpha_h^V, N_h}^{(1D)}(z_h')}{k^2 + \kappa_{nN_e N_h}^2},$$

(47)

with

$$\kappa_{nN_e N_h}^2 = \frac{2\mu}{\hbar^2} \left[ (E_g - \hbar\omega - i\Gamma) + \left( 2n + \frac{3}{2} \right) \hbar\Omega_y \right.$$

$$\left. + \left( N_e + \frac{1}{2} \right) \hbar\Omega_{ez} + \left( N_h + \frac{1}{2} \right) \hbar\Omega_{hz} \right].$$

(48)

The functions $\psi_{\beta, n}^{(1D)}(y)$ are defined in Eq. (40). For further calculations we must specify a trial function $Y$. Accounting only for the lowest confinement state, we use the following trial function:

$$Y = Y_0 \Psi_{00} \psi_{1,\beta}^{(1D)}(y) e^{-\kappa_0 \sqrt{x^2 + y^2}} + \sum_{n=1}^{\infty} \sum_{N_e N_h \geqslant 1} \psi_{2n+1,\beta}^{(1D)}(y)$$

$$\times \Psi_{N_e N_h} \frac{1}{2\pi} \int_{-\infty}^{\infty} dk \, Y_{n N_e N_h}(k) e^{ikx},$$

(49)

where $\kappa_0^2 = \kappa_{000}^2$ and $\Psi_{N_e N_h}$ is defined in Eq. (40); the detailed calculations of $Y_0$ are presented in Appendix D. Then, similarly as in Sec. III C, one can calculate the mean magnetosusceptibility for the Voigt configuration in the intermediate-field regime, arriving at the formula

$$\chi^{\mathrm{interm}V} = \frac{4}{3} \frac{\Delta_{LT}}{R^*} \epsilon_b \left( \frac{a^*}{L} \right) \langle \Psi_{00} \rangle_L \left\{ \frac{1}{\sqrt{\pi}\kappa_0} \rho_0^3 \left( \frac{2\beta}{1 + \beta^2 \rho_0^2} \right)^3 \right.$$

$$\times \exp \left[ \frac{\kappa_0^2 \rho_0^2}{4(1 + \beta^2 \rho_0^2)} \right] D_{-3} \left( \frac{\kappa_0 \rho_0}{\sqrt{1 + \beta^2 \rho_0^2}} \right)$$

$$\times \left. \left[ \frac{2^{3/2}}{\sqrt{\pi}} e^{\kappa_0^2/8\beta^2} D_{-3} \left( \frac{\kappa_0}{\beta\sqrt{2}} \right) - F(\kappa_0, \beta) \right]^{-1} \right.$$

TABLE I. Band parameter values for Cu$_2$O. Masses are given in units of free-electron mass $m_0$. $R^*$ was calculated from $(\mu/\epsilon_b^2) \times 13\,600$ meV. $R_{e,h}^* = (m_{e,h}/\mu)R^*$, and $a_{e,h}^* = (\mu/m_{e,h})a^*$.

| Parameter | Value | Units | Ref. |
|---|---|---|---|
| $E_g$ | 2172.08 | meV | [1] |
| $R^*$ | 87.78 | meV | |
| $\Delta_{LT}$ | $1.25 \times 10^{-3}$ | meV | [24] |
| $m_e$ | 0.99 | $m_0$ | [10] |
| $m_h$ | 0.58 | $m_0$ | [10] |
| $\mu$ | 0.363 | $m_0$ | |
| $M_{\text{tot}}$ | 1.56 | $m_0$ | |
| $a^*$ | 1.1 | nm | [1] |
| $r_0$ | 0.22 | nm | [19] |
| $\epsilon_b$ | 7.5 | | [1] |
| $R_e^*$ | 239.4 | meV | |
| $R_h^*$ | 140.25 | meV | |
| $a_e^*$ | 0.4 | nm | |
| $a_h^*$ | 0.69 | nm | |
| $\Gamma_j$ | $3.88/j^3$ | meV | [1] |

$$+ \sum_{n \geqslant 1, N \geqslant 1} \left\{ \langle \Psi_{NN} \rangle_L \frac{1}{2^{2n}} \left( \frac{\tilde{\beta}}{1 + \tilde{\beta}^2 \rho_0^2} \right)^3 \frac{(2n+1)!}{(n!)^2} \right.$$
$$\left. \times \left( \frac{\tilde{\beta}^2 \rho_0^2 - 1}{\tilde{\beta}^2 \rho_0^2 + 1} \right)^{2n} \frac{\pi}{\kappa_{nN}} w(i \beta \kappa_{nN}) \right\}, \tag{50}$$

where $W_{\kappa,\mu}(z)$ is a Whittaker function of the second kind, $w(z)$ is the complex error function [22], and $F(\kappa_0, \beta)$ is defined in Eq. (D1).

## V. RESULTS

We have calculated the QW magnetoabsorption from the imaginary part of the magnetosusceptibilities, given for the Faraday configuration in Eqs. (23), (28), and (33) and for the Voigt configuration in Eqs. (23) (with appropriate change of parameters), (46), and (50). The parameters used in the calculations are collected in Table I. We assume that the QW band parameters (for example, effective masses) are equal to their bulk values. Since the quantum well thickness under consideration is $L \geqslant 20$ nm, it is much larger than the exciton (1.1 nm for $n = 1$; see Ref. [1]), and the choice of bulk effective masses is justified. The calculations have been performed for the whole spectrum of magnetic field strength, including the weak-, intermediate-, and high-field regimes.

### A. Estimation of regime boundaries

The problem of delimiting boundaries of magnetic field regimes requires a specific analysis for each material. Below we will present simple reasoning which allows for a rough estimation of those limits. The lowest Landau energies for a $p$ exciton (including the Zeeman splitting) given by [see Eq. (27)]

$$U_{0,\pm 1} = \left( \frac{B}{B_{cr}} \right) \left( 2 \pm \frac{\mu}{\mu'} \right) R^* \tag{51}$$

are compared with the two-dimensional hydrogen energy, which for $n = 1$, $m = \pm 1$ is equal to $|4R^*/25|$; thus for $j = 1$ the equation defines the parameter $\gamma_{cr}$

$$\frac{B}{B_{cr}} = \frac{4}{25\left(2 \pm \frac{\mu}{\mu'}\right)} = \gamma_{cr}. \tag{52}$$

This parameter determines the limit of the field: For $B < \gamma_{cr} B_{cr}$, one deals with a weak field; $B \geqslant \gamma_{cr} B_{cr}$ indicates the intermediate-field regime. For the Cu$_2$O data from Table I, depending on the quantum number $m$, we obtain the limiting values 26.8 and 29.2 T. The upper value corresponds to $m = -1$, and the lower one corresponds to $m = 1$. The limiting values of the field decrease with increasing Landau state number $n$.

The limits of the high-field regime in the Faraday configuration can be estimated using the matrix elements given in Eq. (26). Recalling the parameter $\gamma$ given by Eq. (12) and comparing the Landau energy [see Eq. (52)] with the value of the matrix elements

$$W_{11} \approx 4\gamma, \quad |V_{11}| = 1.097\sqrt{\gamma},$$

we obtain the critical value $\gamma_{cr} = 0.075$, which corresponds to a field strength $B$ of about 60 T. Note that this evaluation can be interpreted only as a rough estimation; the real positions of resonances are obtained by solving systems of equations.

In the Voigt configuration, the limits of the weak and intermediate fields can be derived in the same manner as in the Faraday configuration. For a weak field we use the expression (42) and compare with the unperturbed energy values. The Voigt matrix elements are smaller than those for the Faraday one for two reasons. First, in this configuration the magnetic field influences only one degree of freedom [17]. Additionally, the factor $q$ [Eq. (34)], depending on the effective electron and hole masses $v = m_e/m_h$, plays an important role. The function $q(v)$ attains a value of 1 for $v \to 0$, $v \to \infty$ and attains its minimal value for $v = 1$ (as in the "positronium model"). For Cu$_2$O ($v = 1.429$) the parameter $q = 0.273$ approaches that of positronium, so taking the Landau state $n = 1$ and the matrix element $V_{11}$, one obtains the limiting value $\gamma_{cr}$ corresponding to the field strength $B = 56$ T. Comparing this value with the above-indicated limiting values for the Faraday configuration, we see that the limiting values defining the weak-field regime are about twice as large for the Voigt configuration than in the Faraday case. Another related physical effect is that the field-induced blue shift of resonances in the Voigt configuration is much smaller than that in the Faraday configuration; this effect has been experimentally observed [25,26].

The high-field limit for the Voigt configuration will be obtained from the comparison of the Landau energies, which now have the form

$$E_n^V = \left( 2n + \frac{3}{2} \right) \hbar \Omega_y,$$

$$\frac{\hbar \Omega_y}{2R^*} = \frac{\gamma}{2}\sqrt{q} = 0.261\gamma, \quad \hbar \Omega_y = 0.523\,\gamma\,R^*,$$

with the two-dimensional excitonic energies. For the lowest exciton energy $|-4R^*/9|$ we obtain critical magnetic field strengths above 180 T.
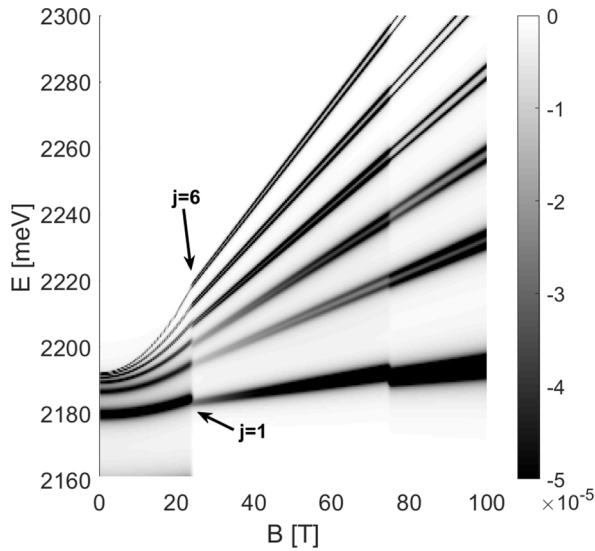
FIG. 1. Imaginary part of the susceptibility (gray scale) of a quantum well in the Faraday configuration, calculated in three field regimes. The lower limits of the intermediate- and high-field regimes are 28 and 75 T, respectively.

As was mentioned above, we are aware that the presented method enables only quantitative estimations, but as will be shown below, the use of parameter $\gamma$ evaluated in such a way gives a good agreement with available experimental data. Having made all the above comments, we present the obtained results.

### B. Discussion of numerical calculations

Figure 1 depicts the absorption spectrum of a Cu₂O quantum well in the Faraday configuration calculated for a range of field strengths $B = 0$–$100$ T and thickness $L = 10$ nm. The boundaries between weak-, intermediate-, and high-field regimes are estimated at 28 and 75 T, which is a close match to the initial estimation of 26.8 (29.2) and 74.49 (81.36) T for $m = +1$ ($m = -1$), respectively. For such values, there is a very good correspondence between solutions [Eqs. (23), (33),

and (28), respectively]. The lines appear in pairs, corresponding to $m = \pm 1$, and exhibit a roughly quadratic energy shift with increasing $B$ in a weak-field limit. Such a tendency has also been observed in bulk samples both experimentally and theoretically [3,7]. Due to the fact that the energy shift of all lines is almost linear for $B > 10$ T, the fit is not sensitive to the changes in low-, medium-, and high-field boundaries, so that even the rough estimations presented above are sufficient to obtain a smooth transition between regimes. It should be pointed out that the mismatch between the $j = 1$ lines originates from the fact that for the lowest state, the two-dimensional Coulomb potential (13) is not a well-justified approximation. However, even for the $j = 2$ state the excitonic wave function is large enough to provide a good match to the results.

Figure 2 depicts the low-field solution calculated for a wide range of quantum numbers $[N, j, m]$, which are given in brackets. It is worth stressing that for QW with REs in a magnetic field those indices describe three types of of states and three origins of resonances; $N$ arises from the confinement in the $z$ direction, the number $j$ enumerating excitons is connected with e-h Coulomb interaction, and $m$ refers to an interaction with the magnetic field resulting in Zeeman splitting with lines shifting towards higher energy with increasing field strength. One can observe several interesting tendencies. By increasing $N$, one introduces an almost constant energy shift (series of blue lines for $j = 2$, orange lines for $j = 3$). On the other hand, the lines coming from higher excitonic states (red series) exhibit a stronger energy shift with increasing $B$ due to stronger sensitivity of higher states to the external field. Finally, the splitting with respect to $m = \pm 1$ is weaker for higher-$j$ lines. This has to do with an intricate situation of interplay between Coulomb and magnetic interactions.

In Fig. 3, one can observe the dependence of the energy shift on the well thickness $L$. As one would expect, the confinement effect is more pronounced for narrow QWs. The states with various $N$ (blue lines) split from the respective $j$ state and diverge as $L \to 0$, with the higher-$N$ states approaching $E \to \infty$ faster due to their lower binding energy and larger physical size, which makes them more affected by finite well size. Higher-$N$ states are more affected by
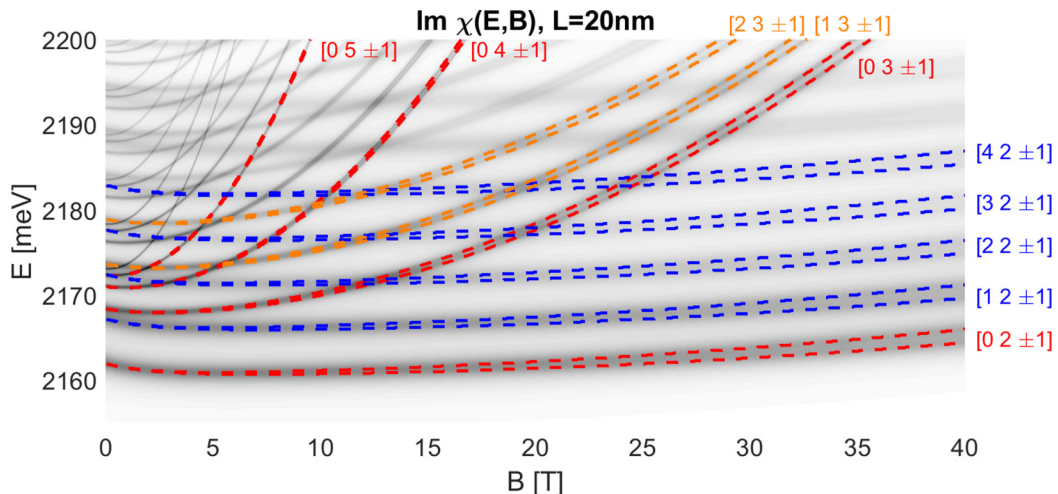


FIG. 2. The same as in Fig. 1, calculated for $L = 20$ nm. The brackets denote quantum numbers $[N, j, m]$.
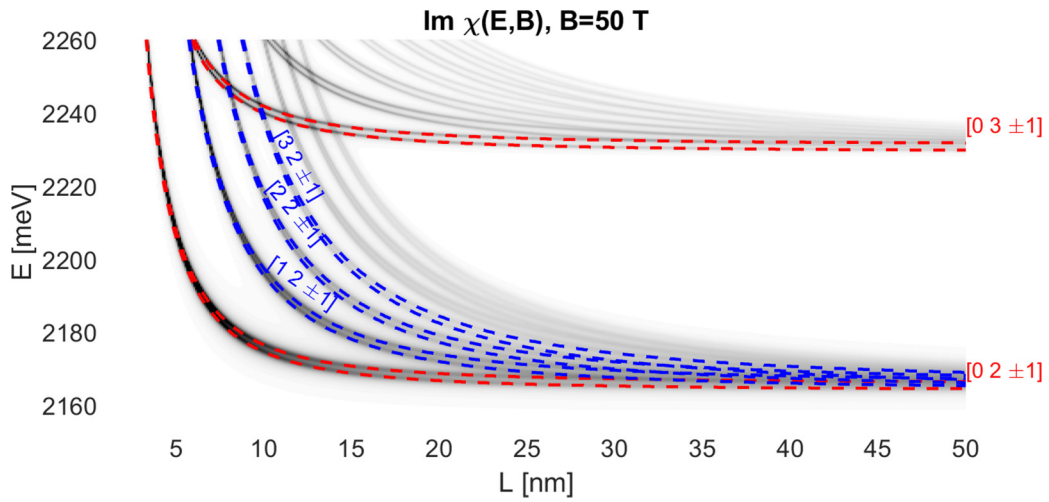
FIG. 3. The same as in Fig. 1, calculated for $B = 50$ T. The brackets denote quantum numbers $[N, j, m]$.

the potential barrier at the quantum well edges. One can observe that the lines with different $j$ (red series) react to the confinement in the same manner—the distance between them remains almost constant up to $L \sim 5$ nm, where the well thickness becomes comparable to the exciton size. The large distance between the $j = 2$ and $j = 3$ states is a result of the high magnetic field ($B = 50$ T); as mentioned before, lines with different $j$ exhibit different energy shifts depending on $B$, which results in increasing distances between them.

The absorption spectrum in the Voigt configuration appears to have a more complicated structure. Figure 4 shows the absorption coefficient calculated from Eq. (23) with Eq. (36) for the weak regime, from Eq. (50) for the intermediate regime, and from Eq. (46) for the strong-field regime. The boundaries between regimes are set to 55 and 140 T. The lower-field limit is equal to the initial estimation, and the high-field limit is

somewhat lower than the initial estimation (180 T), but its exact location is very flexible due to the fact that energy shifts in both intermediate- and strong-field solutions are linear. Again, as in the case of the Faraday configuration, the fit between the two regimes is the best for higher-energy states, which indicates that the presented calculations are particularly suitable for Rydberg excitons. The most striking feature of the spectrum is the grouping of lines corresponding to the same value of $N$, which has the largest contribution to the state energy, especially in the high-field regime. The energy shift depending on other quantum numbers ($m$ and $j$) is less pronounced, so that there are groups of lines centered around the specific value of $N$. In the low-field regime, strong line mixing due to all quantum numbers is visible.

To better discern these states, one can assign the quantum numbers $[N, j, m]$ to them, as shown in Fig. 5. The base state, marked by a red line, is [0,2,0], and the other states are created by changing one quantum number. An increase in $j$ (blue lines) yields a typical, excitonic $\sim 1/j^2$ energy shift, approaching $E = E_g$ at $B = 0$. In our model, the distance between excitonic states is independent of $B$. On the other hand, the energy shift with $B$ depends strongly on $N$ and $m$. Every confinement state $N$ undergoes Zeeman splitting; one can see that the energy of $N = 0$ states with various $m$ (red lines) changes linearly with $B$ and those lines start from a common origin at $B = 0$. The energy shift for higher $N$ (orange lines) is quadratic in the weak-field regime and then turns into linear at $B \sim 50$ T.

The dependence on the well thickness, shown in Fig. 6, is also interesting. One can see that similar to the Faraday configuration, the energies diverge at the very low $L$ limit, with the exact location of the asymptote dependent on the quantum numbers $N$ and $j$ due to the fact that the physical size of an exciton of a given $j$ affects the energy and the magnetic moment of a bound state, which also depends on the quantum number $N$.

We have also performed a comparison of our theoretical results with the available experimental data to verify the accuracy and applicability of our theoretical approach and estimations.
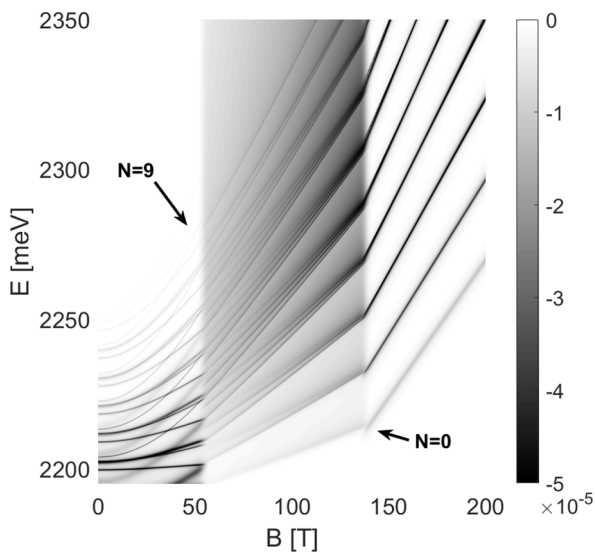


FIG. 4. Imaginary part of susceptibility of a quantum well in the Voigt configuration calculated for a range of magnetic field strengths and $L = 10$ nm.
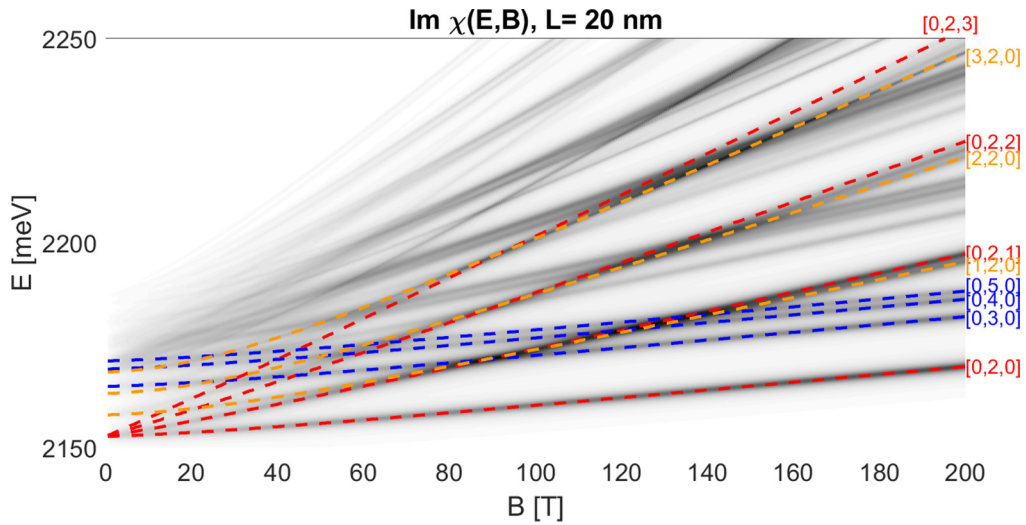
FIG. 5. The same as Fig. 4, with states identified by their quantum numbers $[N, j, m]$.

Figure 7 shows a comparison between the energy of the first confinement $s$ state measured in a GaAlAs quantum dot in the Faraday configuration [25] and the results of our calculations for a Cu$_2$O quantum well, obtained for an $s$ exciton with $m = 0$. For an effective evaluation of two very different systems, relying on the data presented by Wang *et al.* [25], we use the dimensionless parameter $\gamma$ with appropriate Rydberg energies. Furthermore, the significant difference in energy necessitates two $y$ axes to overlap the data. This way, one can observe several similarities. In both systems, the magnetic-field-induced shift is quadratic in the weak-field regime and turns into linear at $\gamma \sim 0.08$, which is consistent with our estimations. It should be stressed that the results are accurate up to a constant; apart from the difference of band gaps and Rydberg energies, the data for GaAlAs are for quantum dots, and our calculations assume cylindrical symmetry. However, as pointed out in Refs. [25] and [9], a proper adjustment of quantum well size allows for an approximation of a quantum dot, which is sufficient for the sake of the presented comparison.

The results for the Voigt configuration are compared with InAlAs in Fig. 8. Again, the estimated boundary between weak- and strong-field regimes provides a good match to the experimental data.

Finally, we use the experimental results of Jeon *et al.* [27] to study the effect of well thickness on the energy, marked by $\Delta E = E(B) - E(0)$ (see Fig. 9). One can observe an increase in the confinement energy with thickness $L$. For any fixed value of $B$, a reduction in $L$ increases the energy (see Fig. 6); however, confinement states in a larger quantum well exhibit a stronger reaction to the magnetic field, which results in higher energy overall.

## VI. CONCLUSIONS

In this paper, we have studied the magneto-optical functions for Cu$_2$O quantum wells with Rydberg excitons at two different orientations of the magnetic field. Theoretical solutions that model absorption spectra due to excitons of Cu$_2$O in a quantum well in a wide range of magnetic fields are
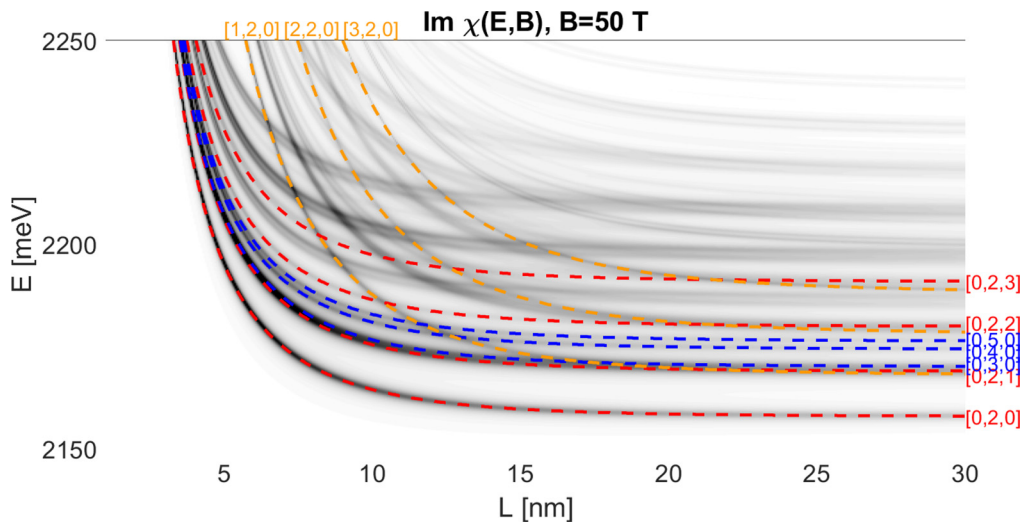


FIG. 6. The same as Fig. 4, calculated for $B = 50$ T and a range of $L$ values, with states identified by their quantum numbers $[N, j, m]$.
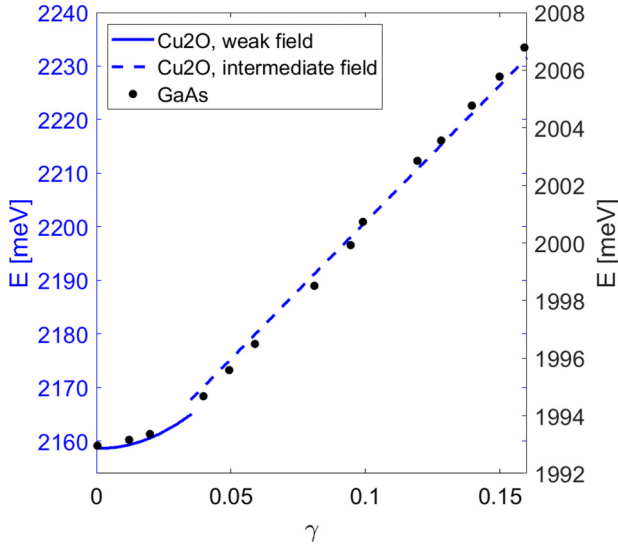
FIG. 7. Comparison of the calculated line shape and experimental results by Wang *et al.* [25] for GaAlAs.



FIG. 9. Comparison of the calculated line shape and experimental results by Jeon *et al.* [27] for a GaAs/AlGaAs quantum well.

presented, with a separate treatment of weak-, intermediate-, and high-field regimes. The theoretical analysis is performed for both Faraday and Voigt external field configurations, including Zeeman splitting. We observe a considerable interlevel mixing and splitting caused by differences in energy shifts of various excitonic states caused by the confinement and the magnetic field. The key characteristics of $Cu_2O$ excitons—an unusually high Rydberg energy, an exceptionally large size of higher states, and a unique ratio of electron mass to hole mass—play a crucial role in forming rich magnetic absorption spectra. We conclude that in QW the difference between the spectra obtained in both configurations depends on degrees of freedom involved in the interaction between the excitons and the magnetic field. Because of that and because of an effective electron-mass-to-hole-mass ratio we
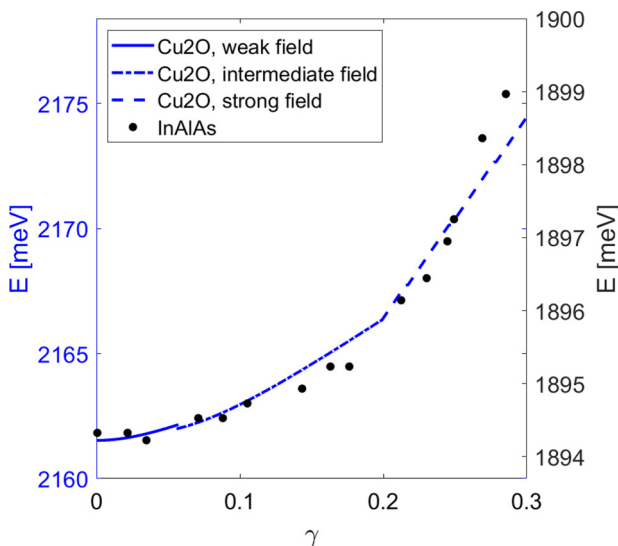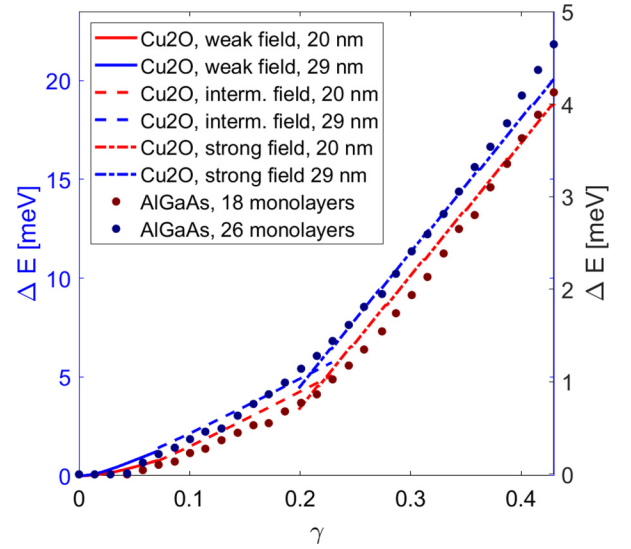
observe that the boundaries of the intermediate- and high-field regimes are significantly higher for the Voigt configuration.

Finally, we introduce a field-dependent parameter $\gamma$ which is a versatile tool for qualitative separation of the magnetic field regimes. Due to its universal nature, it can be employed to compare the calculation results with experimental spectra measured in other semiconductors, serving as a benchmark of this paper.

### APPENDIX A: MATRIX ELEMENTS

We calculate the matrix elements (22) using the eigenfunctions (17). First, we calculate the diagonal elements

$$
\begin{aligned}
V_{jj} &= \frac{\gamma^2}{4} \langle R_{j1}(\rho) | \rho^2 | R_{j1}(\rho) \rangle \\
&= \frac{\gamma^2}{4} 16\lambda^3 \left[ \frac{j!}{(j+2|m|)!} \right] \int_0^\infty \rho \, d\rho \, e^{-4\lambda\rho} (4\lambda\rho)^2 \rho^2 \\
&\quad \times \left[ L_j^2(4\lambda\rho) \right]^2 \\
&= \frac{\gamma^2}{64\lambda(j+1)(j+2)} \int_0^\infty dx \, e^{-x} x^4 \left[ x L_j^2(x) \right] L_j^2(x). \quad \text{(A1)}
\end{aligned}
$$

The integral in the above equation is known [28], and we obtain the expression

$$
\begin{aligned}
V_{jj1} &= \frac{\gamma^2 (j+2)!}{64\lambda(j+1)(j+2)} 4! \left\{ (2j+3)(j+2)! \left[ \frac{1}{j!2!} \right]^2 \right. \\
&\quad \left. + \frac{(j+3)!}{[j!]^2 3!} + \frac{(j+1)(j+2)}{(j-1)!3!} \right\}. \quad \text{(A2)}
\end{aligned}
$$



FIG. 8. Comparison of the calculated line shape and experimental results by Wang *et al.* [25] for InAlAs.

The off-diagonal elements can be obtained using Rodrigues's formula

$$L_j^\alpha(x) = \sum_{\ell=0}^{j} (-1)^\ell \binom{j+\alpha}{j-\ell} \frac{x^\ell}{\ell!}. \tag{A3}$$

Performing the integration, we obtain the matrix elements in the form

$$V_{ij1} = \frac{\gamma^2}{4} \int_0^\infty \rho \, d\rho R_{i1}(\rho) \, \rho^2 \, R_{j1}(\rho)$$

$$= 4^3 \gamma^2 (\lambda_i \lambda_j)^{5/2} \left[ \left( \frac{i!}{(i+2)!} \right) \left( \frac{j!}{(j+2)!} \right) \right]^{1/2}$$

$$\times \sum_{r=0}^{i} \sum_{s=0}^{j} \left\{ \binom{i+2}{i-r} \binom{j+2}{j-s} \frac{(-1)^{r+s}}{r!s!} \right.$$

$$\left. \times (4\lambda_i)^r (4\lambda_j)^s \frac{(5+r+s)!}{[2(\lambda_i+\lambda_j)]^{5+r+s+1}} \right\}. \tag{A4}$$

Using formula (A3) above, we calculated the matrix elements $V_{n\ell m}$ for the high-field limit (26). After simple transformations, for the case $|m| = 1$, they can be put into the form

$$V_{jk1} = -\frac{2\sqrt{2\gamma}}{\sqrt{(j+1)(k+1)}} \int_0^\infty dx \, e^{-x^2} x^2 \, L_j^1(x^2) L_k^1(x^2),$$

from which one obtains the formula

$$V_{jk1} = -\frac{1}{\sqrt{(j+1)(k+1)}} \sqrt{\frac{\pi\gamma}{2}} \sum_{r=0}^{j} \sum_{s=0}^{k} \binom{j+1}{j-r}$$

$$\times \binom{k+1}{k-s} \frac{(-1)^{r+s}}{r!s!} \frac{(2r+2s+1)!!}{2^{r+s}}. \tag{A5}$$

## APPENDIX B: INTERMEDIATE FIELDS, FARADAY CONFIGURATION

Substituting the trial function (31) into the Eq. (29), with $V = -2/\rho$, one obtains the following integral equation:

$$\Psi_{00} R_{01}(\rho) \left[ \sum_{m=\pm 1} Y_{0m,00} \exp(-\kappa_{0m00}\rho) \frac{e^{im\phi}}{\sqrt{2\pi}} \right] + \sum_{n=1}^\infty \sum_{N_e N_h \geqslant 1} \sum_m \frac{e^{im\phi}}{\sqrt{2\pi}} Y_{nmN_eN_h} R_{nm}(\rho) \Psi_{N_eN_h}$$

$$= \frac{2\mu}{\hbar^2 a^*} \left[ (M_0\rho_0) \frac{2\gamma}{\sqrt{\pi}} \right] \frac{e^{i\phi}}{\sqrt{2\pi}} \sum_{n=0}^\infty R_{n1}(\rho) \frac{d_{n1}}{\kappa_{n1;N_eN_h}^2} + \frac{2\mu}{\hbar^2 a^*} \left[ (M_0\rho_0) \frac{2\gamma}{\sqrt{\pi}} \right] \frac{e^{-i\phi}}{\sqrt{2\pi}} \sum_{n=0}^\infty R_{n1}(\rho) \frac{d_{n1}}{\kappa_{n,-1;N_eN_h}^2} + \int_0^\infty \rho' d\rho' \int_0^{2\pi} d\phi'$$

$$\times \int_{-\infty}^\infty dz_e' \int_{-\infty}^\infty dz_h' \left\{ G(\rho, \rho'; \phi, \phi'; z_e, z_e'; z_h, z_h') \frac{2}{\rho'} R_{01}(\rho') \Psi_{00}(z_e', z_h') \left[ \sum_{m=\pm 1} Y_{0m;00} \frac{\exp(-\kappa_{0m;00}\rho')}{\kappa_{nm;N_eN_h}^2} \frac{e^{im\phi'}}{\sqrt{2\pi}} \right] \right\}. \tag{B1}$$

From various methods of solving integral equations we choose the method of projection on an orthonormal basis $u_{nm}(\rho, \phi)$, $\Psi_{N_eN_h}(z_e, z_h)$. We can use the functions $\psi_{nm}(\rho) \exp(im\phi)/\sqrt{2\pi}$ to obtain

$$Y_{0m,00} \langle R_{01}^2 | e^{-\kappa_{0m;00}\rho} = \frac{2\mu}{\hbar^2 a^*} \left[ (M_0\rho_0) \frac{2\gamma}{\sqrt{\pi}} \right] \mathcal{E} \frac{d_{01}}{\kappa_{0m;00}^2} + 2 \sum_{m=\pm 1} Y_{0m,00} \int_0^\infty d\rho' \frac{e^{-\kappa_{0m;00}\rho'}}{\kappa_{0m;00}^2} R_{01}^2(\rho'). \tag{B2}$$

From the above equation the parameters $Y_{0m,00}$ and $Y_{nm,00}$ were obtained.

## APPENDIX C: THE COEFFICIENTS FOR THE ADIABATIC POTENTIALS

The coefficients $a_{2n+1}$ are defined from the relations

$$\langle \psi_{\beta,N_y}^{(1D)}(y) | \frac{2}{\sqrt{x^2+y^2}} | \psi_{\beta,N_y}^{(1D)}(y) \rangle = \frac{2}{|x| + a_{N_y}}, \quad \frac{1}{a_{N_y}} = \langle \psi_{\beta,N_y}^{(1D)}(y) | \frac{2}{\sqrt{x^2+y^2}} | \psi_{\beta,N_y}^{(1D)}(y) \rangle \bigg|_{x=0}.$$

For odd-parity eigenfunctions, $N_y = 2n + 1$, and we use the relation between Hermite polynomials and the confluent hypergeometric function

$$\psi_{2n+1,\beta}^{(1D)}(y) = A_{2n+1} H_{2n+1}(\beta y) e^{-\beta^2 y^2/2}$$

$$= A_{2n+1}(-1)^n \, 2 \frac{(2n+1)!}{n!} \beta y \, M\left(-n, \frac{3}{2}, \beta^2 y^2\right) e^{-\beta^2 y^2/2}, \tag{C1}$$

with the normalization factor $A_{2n+1}$. The coefficients $a_{2n+1}$ are obtained from the following calculations:

$$
\begin{aligned}
\frac{1}{a_{2n+1}} &= 2\int_0^\infty \left[\psi_{2n+1,\beta}^{(1D)}\right]^2 \frac{1}{y} dy \\
&= 2[A_{2n+1}]^2 \int_0^\infty \left[\frac{(2n+1)!}{n!}\right]^2 4\left[M\left(-n,\frac{3}{2},\beta^2 y^2\right)\right]^2 e^{-\beta^2 y^2}\beta^2 y\, dy \\
&= \pi^{-1/2}\frac{\beta(2n+1)!}{2^{2n+1}(n!)^2}4\int_0^\infty e^{-z}\left[M\left(-n,\frac{3}{2},z\right)\right]^2 dz \\
&= \pi^{-1/2}\frac{\beta(2n+1)!}{2^{2n-1}(n!)^2}J_1^n.
\end{aligned}
\tag{C2}
$$

We use the integral [29]

$$
J_\nu^n = \int_0^\infty e^{-kz}z^{\nu-1}[M(-n,\gamma,kz)]^2 dz.
$$

For $n=0$,

$$
J_\nu^0 = \frac{1}{k^\nu}\Gamma(\nu).
$$

For $n = 1, 2, \ldots,$

$$
\begin{aligned}
J_\nu^n &= \frac{\Gamma(\nu)n!}{k^\nu\gamma(\gamma+1)\cdots(\gamma+n-1)}\left\{1+\frac{n(\gamma-\nu-1)(\gamma-\nu)}{1^2\cdot\gamma}+\frac{n(n-1)(\gamma-\nu-2)(\gamma-\nu-1)(\gamma-\nu)(\gamma-\nu+1)}{1^2\cdot 2^2\cdot\gamma(\gamma+1)}+\cdots\right. \\
&\left.\quad+\frac{n(n-1)\cdots 1(\gamma-\nu-n)\cdots(\gamma-\nu+n-1)}{1^2\cdots n^2\cdot\gamma(\gamma+1)\cdots(\gamma+n-1)}\right\}.
\end{aligned}
$$

In our case we set $k=1$, $\nu=1$, $\gamma=\frac{3}{2}$. For the lowest values of $n$, one obtains

$$
\begin{aligned}
n=0, \quad J_1^0 &= 1, \quad \frac{1}{a_1} = \pi^{-1/2}\cdot 2\beta, \quad a_1 = \frac{1}{2}\sqrt{\pi}\beta^{-1}, \\
n=1, \quad J_1^1 &= \frac{5}{9}, \quad \frac{1}{a_3} = \pi^{-1/2}\cdot\frac{5\beta}{3}, \quad a_3 = \frac{3}{5}\sqrt{\pi}\beta^{-1}, \\
n=2, \quad J_1^2 &= \frac{2}{5}, \quad \frac{1}{a_5} = \pi^{-1/2}\cdot\frac{3}{2}\beta, \quad a_5 = \frac{2}{3}\sqrt{\pi}\beta^{-1}.
\end{aligned}
$$

## APPENDIX D: DETERMINATION OF PARAMETERS FOR INTERMEDIATE FIELDS IN THE VOIGT CONFIGURATION

Inserting the trial function (49) into Eq. (30) and using the Green's function (47), one obtains an equation from which, retaining the lowest expansion term in $GVY$, one obtains the following expression:

$$
\begin{aligned}
&Y_0\Psi_{00}(z_e,z_h)\psi_{1,\beta}^{(1D)}(y)e^{-\kappa_0\sqrt{x^2+y^2}}+\sum_{n=1}^\infty\sum_{N_eN_h\geqslant 1}\psi_{2n+1,\beta}^{(1D)}(y)\Psi_{N_eN_h}(z_e,z_h)\frac{1}{2\pi}\int_{-\infty}^\infty dk\, Y_{nN_eN_h}(k)e^{ikx} \\
&= \frac{2\mu}{\hbar^2 a^*}\mathcal{E}\frac{(M_0\rho_0)}{\sqrt{2\pi}}\sum_n\sum_{N_e}\sum_{N_h}g_{2n+1}\psi_{2n+1,\beta}^{(1D)}(y)\Psi_{N_eN_h}(z_e,z_h)\delta_{N_eN_h}\int_{-\infty}^\infty\frac{dk\, e^{ikx}\,e^{-k^2\rho_0^2/2}}{k^2+\kappa_{nN_eN_h}^2} \\
&\quad+4Y_0\sum_{n,N_e,N_h}\int_{-\infty}^\infty dz_e'\int_{-\infty}^\infty dz_h'\frac{1}{2\pi}\int_0^\infty dx'\int_{-\infty}^\infty dy'\int_{-\infty}^\infty dk\, e^{ikx}\cos kx'\,\psi_{\beta,n}^{(1D)}(y)\psi_{\beta,n}^{(1D)}(y') \\
&\quad\times\frac{\psi_{\alpha_e^V,N_e}^{(1D)}(z_e)\psi_{\alpha_e^V,N_e}^{(1D)}(z_e')\psi_{\alpha_h^V,N_h}^{(1D)}(z_h)\psi_{\alpha_h^V,N_h}^{(1D)}(z_h')}{k^2+\kappa_{nN_eN_h}^2}\frac{\exp(-\kappa_0\sqrt{x'^2+y'^2})}{\sqrt{x'^2+y'^2}}\psi_{\beta,1}^{(1D)}(y')\Psi_{00}(z_e'z_h').
\end{aligned}
$$

A similar equation was obtained in Appendix B, and it was solved by making projections on an orthonormal set of functions. Here, we choose the functions $\{\psi_{\beta,n}^{(1D)}(y)\}$, $\Psi_{N_e N_h}$, set $x = 0$, and obtain

$$Y_0 = \frac{2\mu}{\hbar^2 a^*}\mathcal{E}\frac{(M_0\rho_0)}{\sqrt{\pi}}\frac{g_1}{\kappa_0}\left[\frac{2^{3/2}}{\sqrt{\pi}}e^{\kappa_0^2/8\beta^2}D_{-3}\left(\frac{\kappa_0}{\beta\sqrt{2}}\right) - F(\kappa_0,\beta)\right]^{-1},$$

$$F(\kappa_0,\beta) = \frac{\beta}{\sqrt{\pi}}\int_{-\infty}^{\infty}dk\,\frac{e^{-k^2\rho_0^2/2}}{(k^2+\kappa_0^2)^{3/2}}\exp\left(\frac{k^2+\kappa_0^2}{8\beta^2}\right)W_{-1,0}\left(\frac{k^2+\kappa_0^2}{4\beta^2}\right),$$

$$\frac{1}{2\pi}Y_{nN}(k) = \frac{2\mu}{\hbar^2 a^*}\mathcal{E}\frac{M_0\rho_0}{\sqrt{2\pi}}g_{2n+1}\frac{e^{-k^2\rho_0^2}}{k^2+\kappa_{nN}^2}.$$

The above quantities, substituted into Eq. (49), determine the exciton amplitude $Y$, which, inserted into Eq. (20), gives the magnetosusceptibility (50).

---

[1] T. Kazimierczuk, D. Fröhlich, S. Scheel, H. Stolz, and M. Bayer, Nature (London) **514**, 344 (2014).

[2] M. Aßmann and M. Bayer, Adv. Quantum Technol. **3**, 1900134 (2020).

[3] P. Rommel, F. Schweiner, J. Main, J. Heckötter, M. Freitag, D. Fröhlich, K. Lehninger, M. Aßmann, and M. Bayer, Phys. Rev. B **98**, 085206 (2018).

[4] J. Thewes, J. Heckötter, T. Kazimierczuk, M. Aßmann, D. Fröhlich, M. Bayer, M. A. Semina, and M. M. Glazov, Phys. Rev. Lett. **115**, 027402 (2015).

[5] F. Schöne, S.-O. Krüger, P. Grünwald, H. Stolz, S. Scheel, M. Aßmann, J. Heckötter, J. Thewes, D. Fröhlich, and M. Bayer, Phys. Rev. B **93**, 075203 (2016).

[6] F. Schweiner, J. Main, G. Wunner, M. Freitag, J. Heckotter, C. Uihlein, M. Aßmann, D. Frohlich, and M. Bayer, Phys. Rev. B **95**, 035202 (2017).

[7] S. Zielińska-Raczyńska, D. Ziemkiewicz, and G. Czajkowski, Phys. Rev. B **95**, 075204 (2017).

[8] S. Zielinska-Raczyńska, D. A. Fishman, C. Faugeras, M. M. P. Potemski, P. H. M. van Loosdrecht, K. Karpiński, G. Czajkowski, and D. Ziemkiewicz, New J. Phys. **21**, 103012 (2019).

[9] D. Ziemkiewicz, K. Karpiński, G. Czajkowski, and S. Zielińska-Raczyńska, Phys. Rev. B **101**, 205202 (2020).

[10] N. Naka, I. Akimoto, M. Shirai, and K.-i. Kan'no, Phys. Rev. B **85**, 035209 (2012).

[11] M. Takahata, K. Tanaka, and N. Naka, Phys. Rev. B **97**, 205305 (2018).

[12] A. Konzelmann, B. Frank, and H. Giessen, J. Phys. B: At., Mol. Opt. Phys. **53**, 024001 (2020).

[13] F. Katsch, D. Christiansen, R. Schmidt, S. Michaelis de Vasconcellos, R. Bratschitsch, A. Knorr, and M. Selig, Phys. Rev. B **102**, 115420 (2020).

[14] A. Stahl and I. Balslev, *Electrodynamics of the Semiconductor Band Edge* (Springer, New York, 1987).

[15] D. Merbach, E. Schöll, W. Ebeling, P. Michler, and J. Gutowski, Phys. Rev. B **58**, 10709 (1998).

[16] D. Merbach, E. Schöll, and J. Gutowski, J. Appl. Phys. (Melville, NY) **85**, 7051 (1999).

[17] G. Czajkowski, F. Bassani, and L. Silvestri, Riv. del Nuovo Cimento **026**, 1 (2003).

[18] P. L. Valdés-Negrin, B. Flores-Desirena, M. Toledo-Solano, and F. Pérez-Rodriguez, AIP Adv. **10**, 065223 (2020).

[19] S. Zielińska-Raczyńska, G. Czajkowski, and D. Ziemkiewicz, Phys. Rev. B **93**, 075206 (2016).

[20] J. Heckötter, D. Frölich, M. Aßmann, and M. Bayer, Phys. Solid State **60**, 1595 (2018).

[21] D. Ziemkiewicz, G. Czajkowski, K. Karpiński, and S. Zielińska-Raczyńska, arXiv:2009.13621 v1[cond-mat.mes-hall].

[22] M. Abramowitz and I. Stegun, *Handbook of Mathematical Functions* (Dover, New York, 1965).

[23] N. F. Mott and H. S. W. Masey, *The Theory of Atomic Collisions* (Clarendon, Oxford, 1965).

[24] H. Stolz, F. Schöne, and D. Semkat, New J. Phys. **20**, 023019 (2018).

[25] P. D. Wang, J. L. Merz, S. Fafard, R. Leon, D. Leonard, G. Medeiros-Ribeiro, M. Oestreich, P. M. Petroff, K. Uchida, N. Miura, H. Akiyama, and H. Sakaki, Phys. Rev. B **53**, 16458 (1996).

[26] A. V. Chernenko, P. S. Dorozhkin, V. D. Kulakovskii, A. S. Brichkin, S. V. Ivanov, and A. A. Toropov, Phys. Rev. B **72**, 045302 (2005).

[27] M. H. Jeon, K. H. Yooa, M. G. Sung, I. T. Jeong, J. C. Woo, and L. R. Ram-Mohan, Solid State Commun. **150**, 1782 (2010).

[28] I. S. Gradshteyn and I. M. Ryzhik, in *Table of Integrals, Series, and Products*, 7th ed., edited by A. Jeffrey and D. Zwillinger (Elsevier, Amsterdam, 2007).

[29] L. D. Landau and E. M. Lifshitz, *Quantum Mechanics* (Pergamon, Oxford, 1963).